nature energy

Article

https://doi.org/10.1038/s41560-023-01280-1

# High-entropy electrolytes for practical lithium metal batteries

In the format provided by the authors and unedited

**Supplementary Figures**

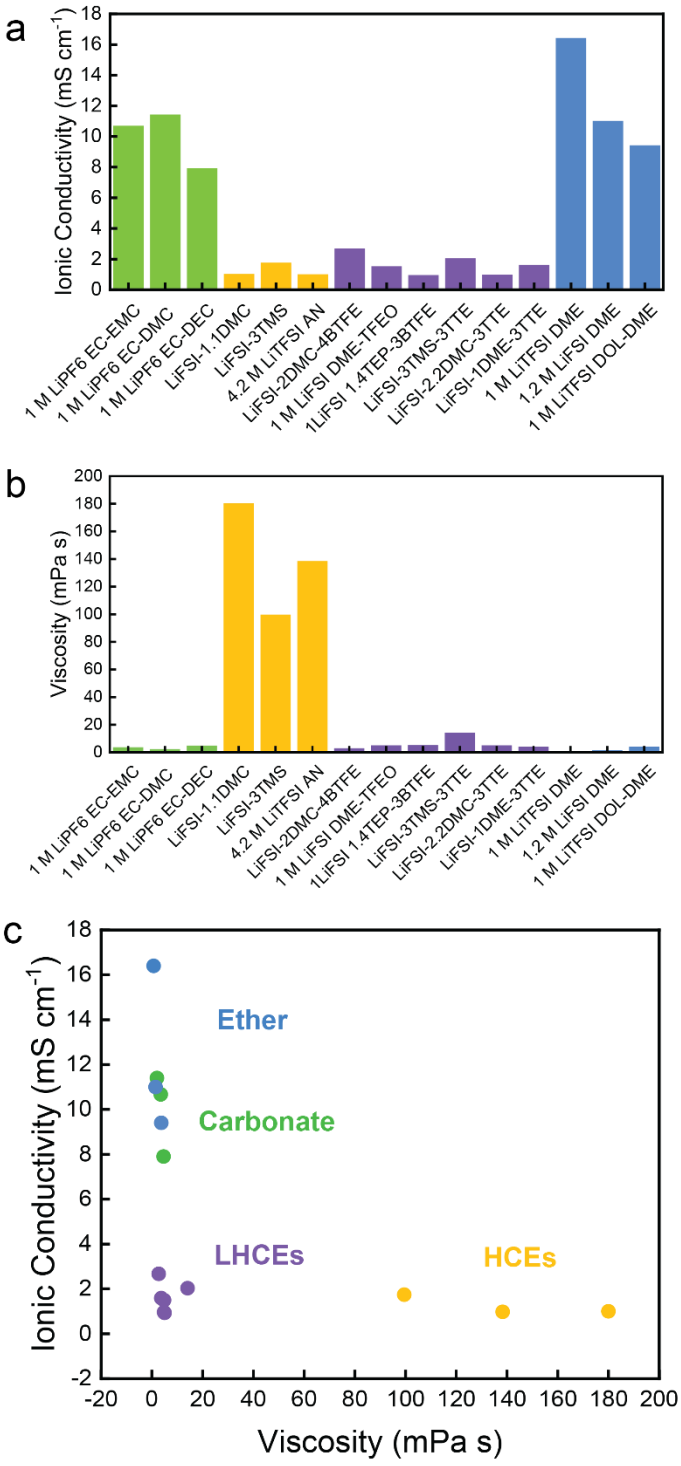


Supplementary Fig. 1: Ionic conductivity and viscosity values from the literature, where the references are given in Supplementary Table 1.

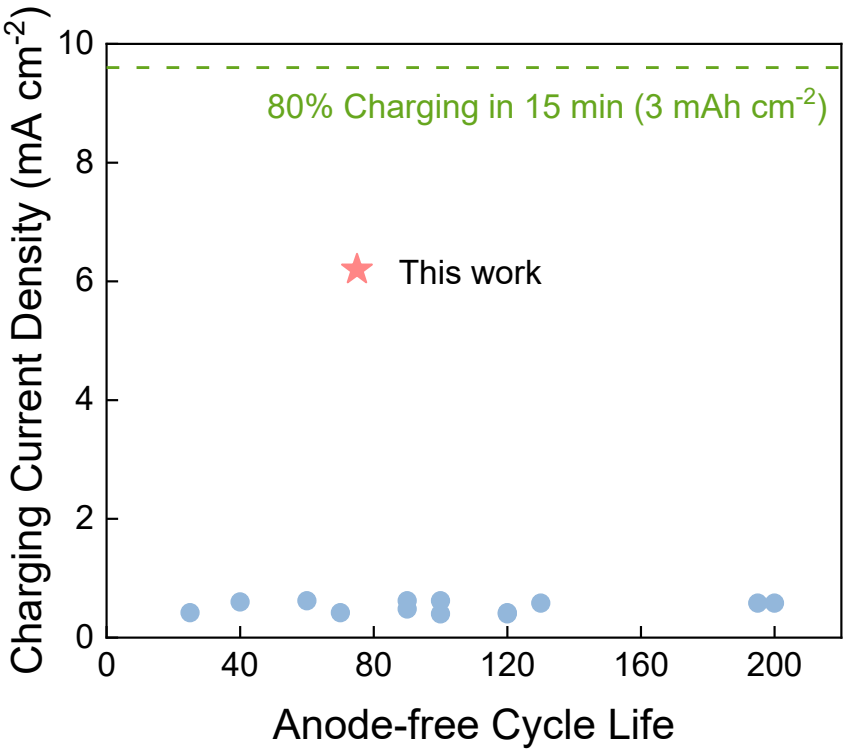


Supplementary Fig. 2: Reported anode-free cell cycle life and current density values from the literature, where the references are given in Supplementary Table 2.

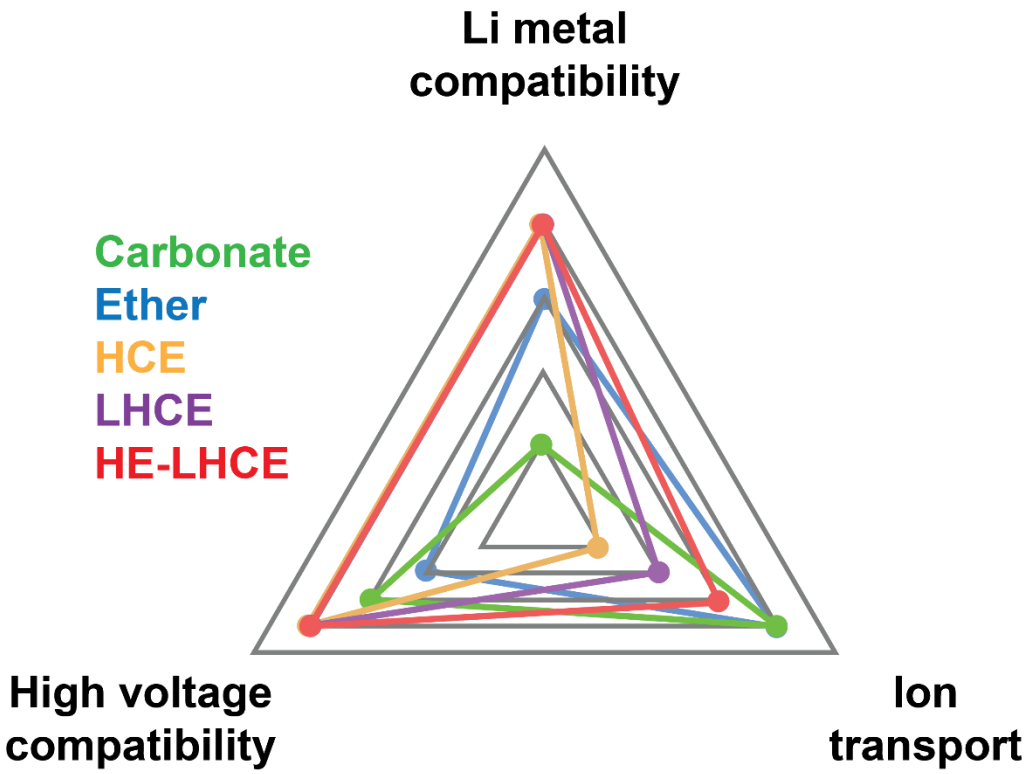


Supplementary Fig. 3: Summary of high voltage compatibility, Li metal compatibility and ion transport capabilities of various electrolytes.

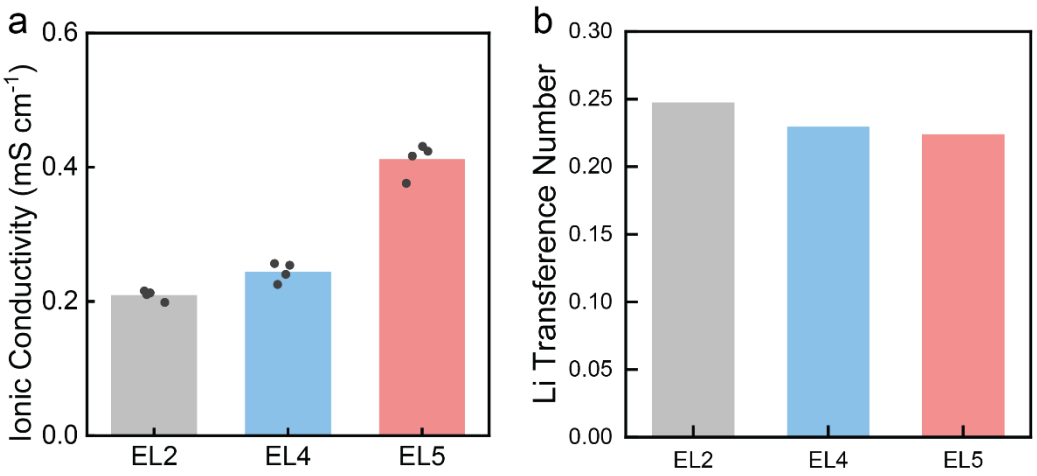


Supplementary Fig. 4: Ionic conductivities and transference numbers of the EL2-EL5 measured with separators in coin cells, where clear differences in conductivity can be seen while transference numbers are similar across electrolytes. Conductivities with separators were measured as ion transport through separator pores can have different behavior from bulk solution, depending on wettability and surface energy. Li transference number is similar across electrolytes, which infers that the mobility of both $Li^+$ and anions are increased with increasing molecular diversity.

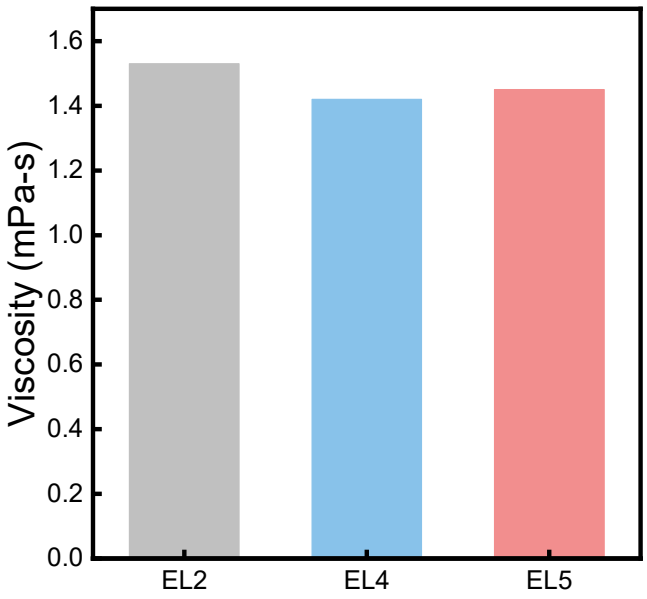


Supplementary Fig. 5: Viscosities of the three electrolytes are similar.

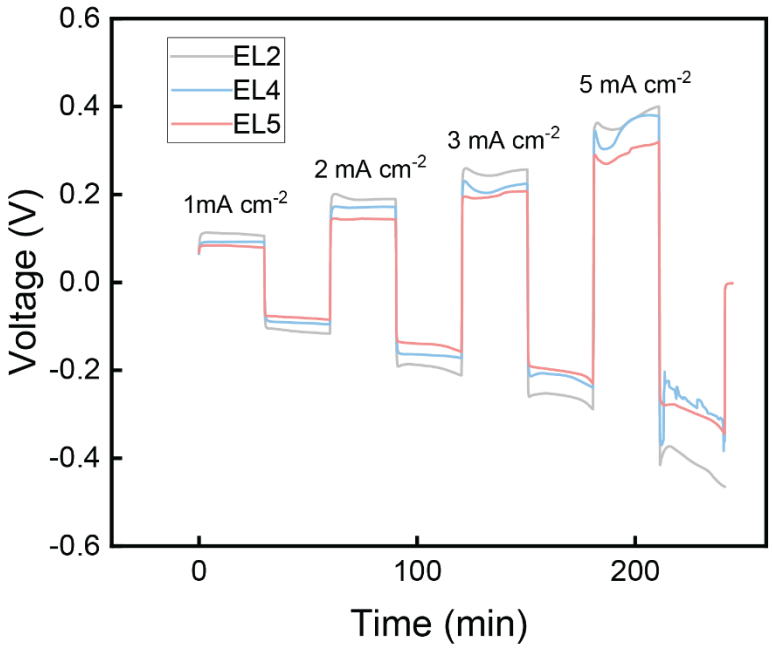


Supplementary Fig. 6: Voltage profiles of Li || Li cycling at various current densities, showing decreasing overpotential in the order of EL2-EL4-EL5.

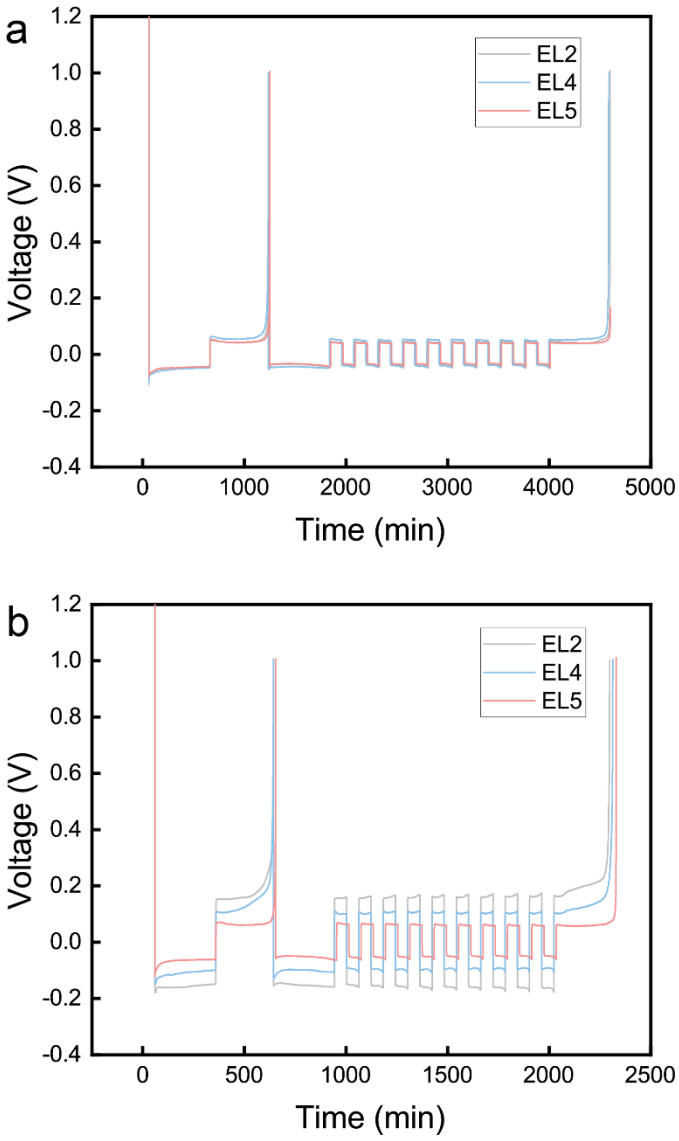


Supplementary Fig. 7: Li || Cu Coulombic efficiency measurements of EL2-EL5 using the Aurbach method at a) 0.5 mA $cm^{-2}$ and b) 1 mA $cm^{-2}$.

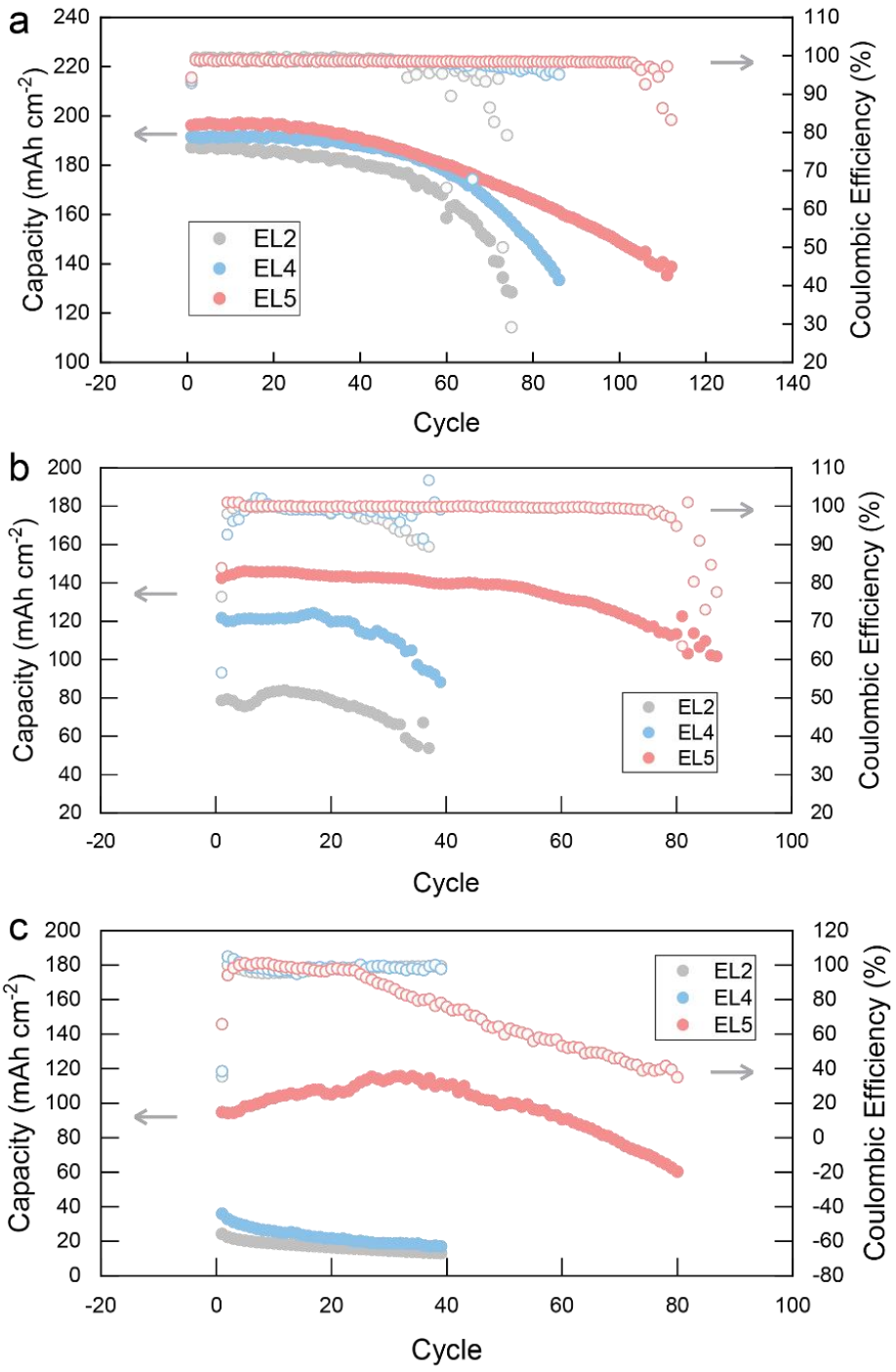


Supplementary Fig. 8: Capacity and Coulombic efficiency of anode-free NMC532-Cu pouch cell cycling at 3.0-4.4V cycled at a, 0.2C charging and 0.5C discharging. b, 1C charging and 1.5C discharging. c, 2C charging and discharging.

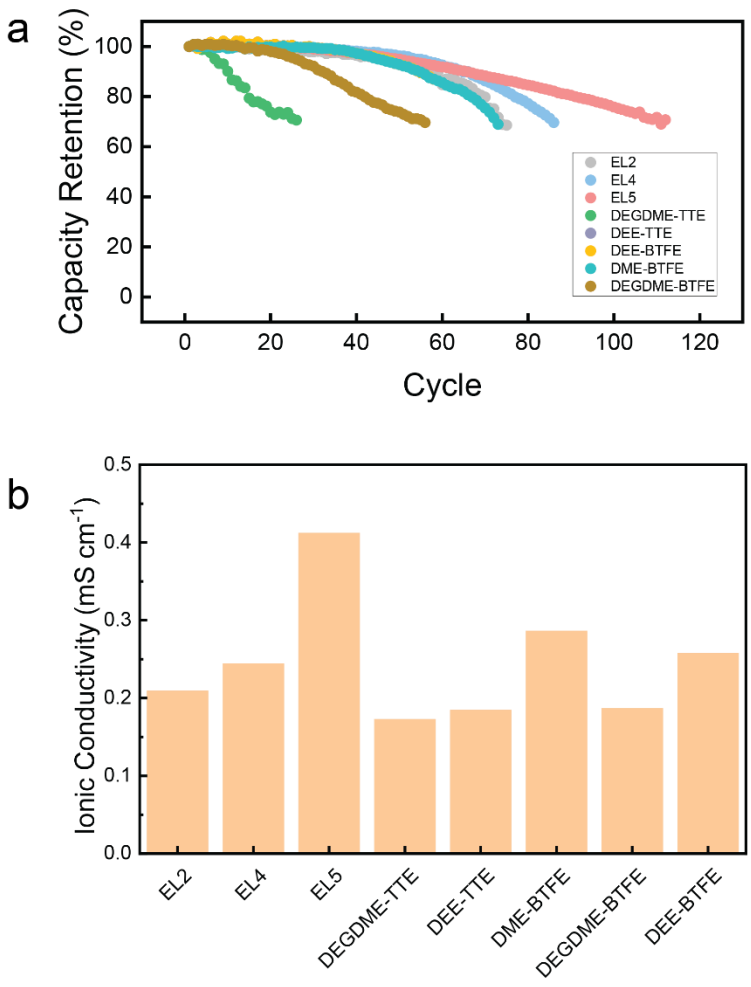


Supplementary Fig. 9: a) NMC532-Cu pouch cell cycling and b) ionic conductivities of various combinations of electrolytes, where EL5 shows performance significantly exceeding the average performance of all electrolytes.

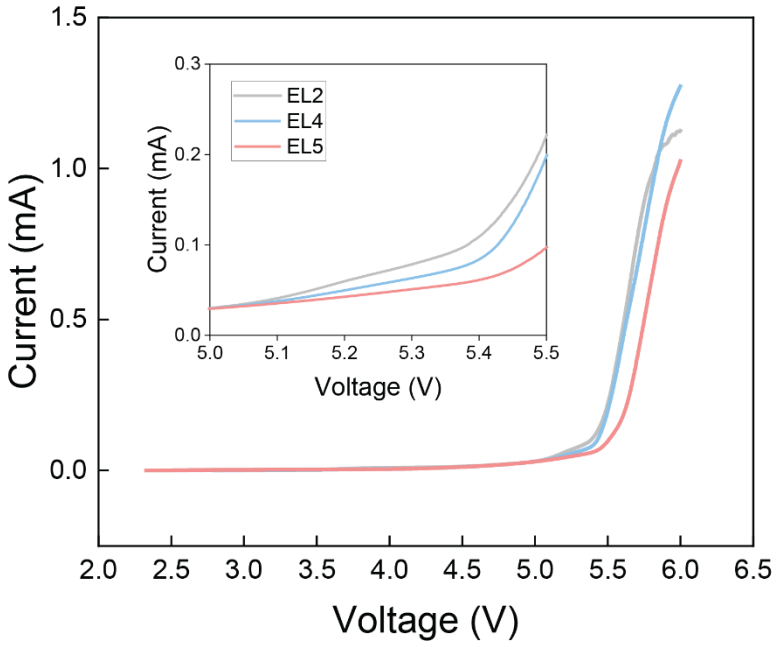


Supplementary Fig. 10: Linear sweep voltammetry (LSV) of the EL2-EL5 electrolytes, where oxidative stability slightly improves in the order of EL2-EL4-EL5.

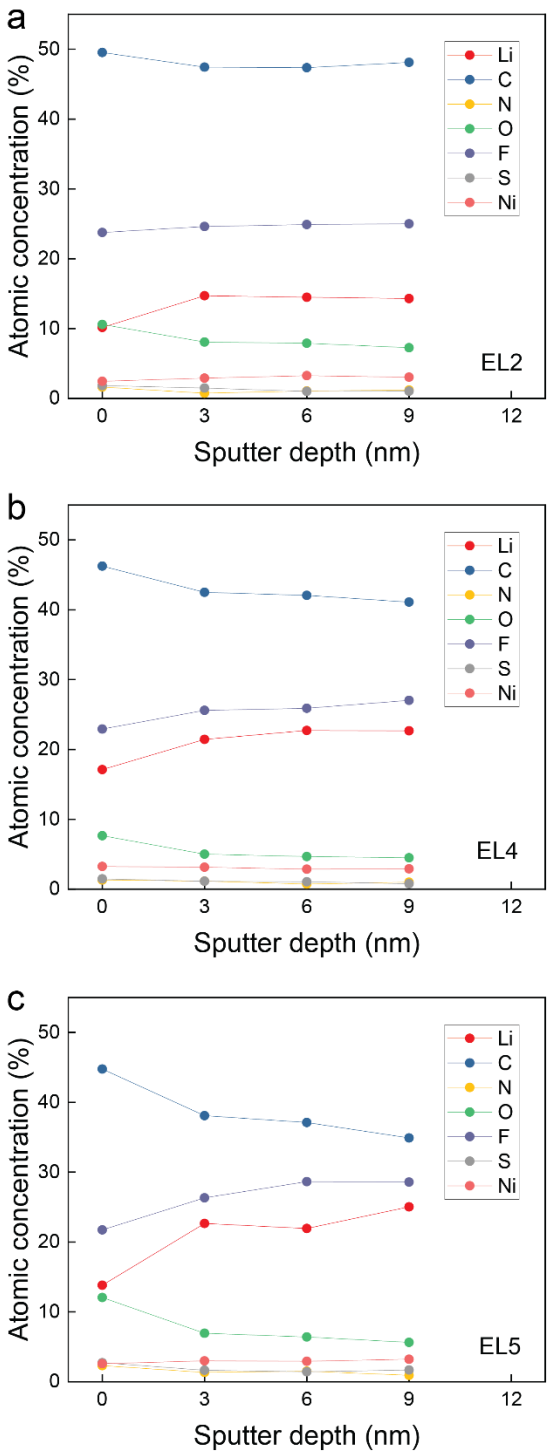


Supplementary Fig. 11: XPS characterization of the NMC532 CEI after 50 cycles in different electrolytes, showing while the interphase chemistries are similar, fluorine content increases and carbon content decreases in the order of EL2-EL4-EL5. The points represent the mean of 3 different spots.

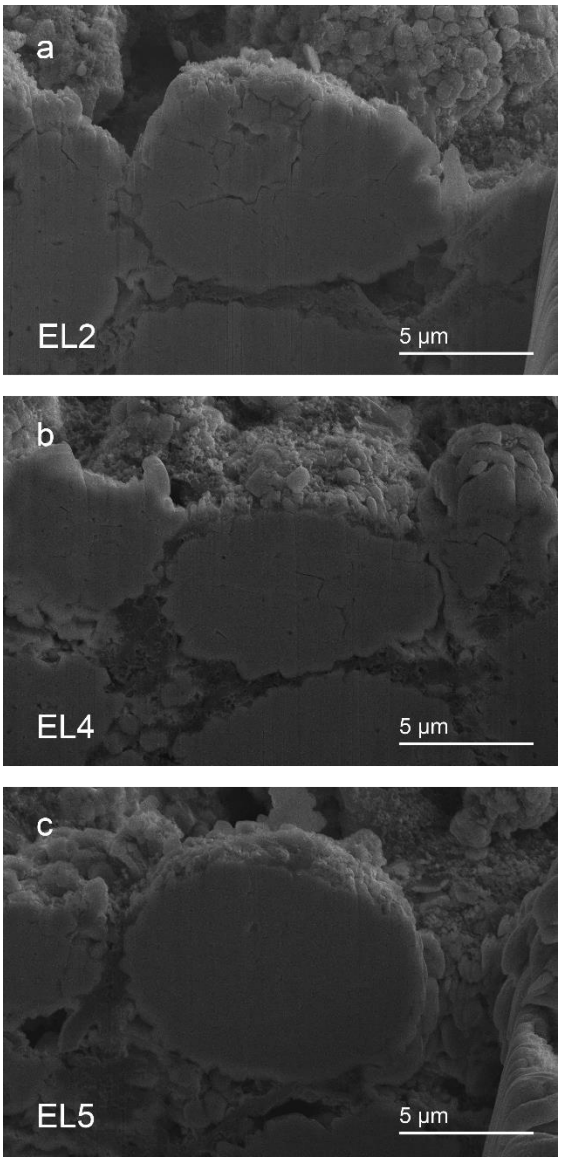


Supplementary Fig. 12: FIB-SEM images of NMC532 cathode particles after 50 cycles using different electrolytes, showing that while all samples retain relatively good structural integrity, crack formation decreases in the order of EL2-EL4-EL5.

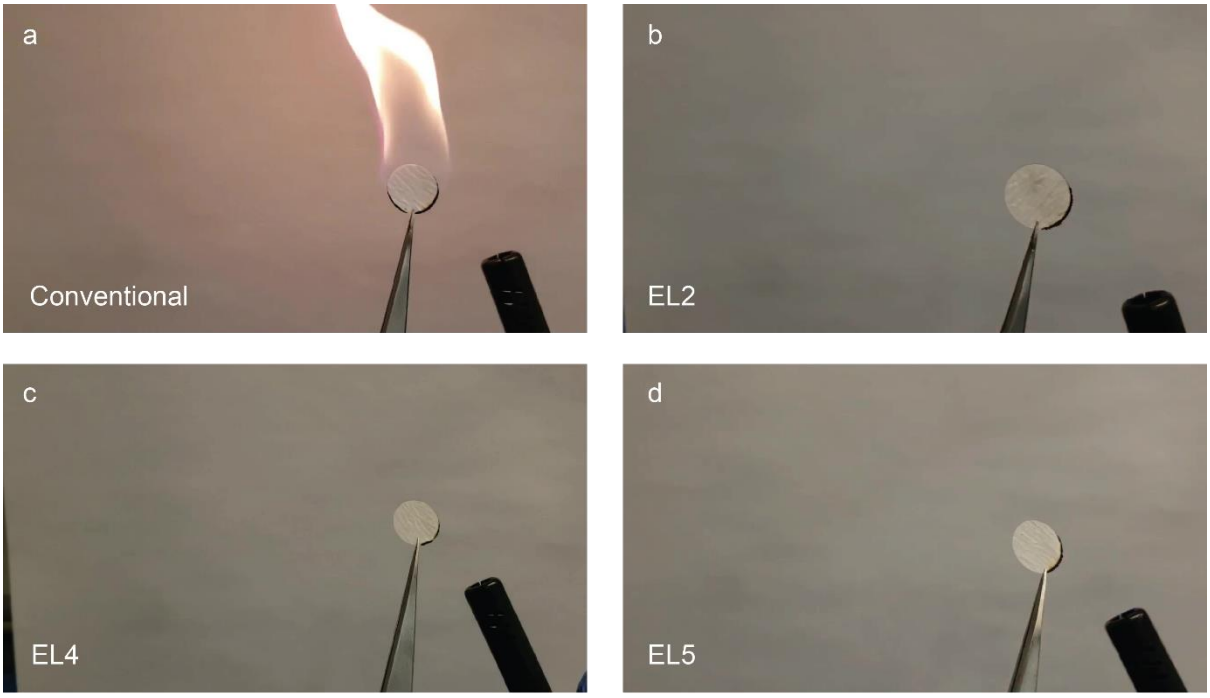


Supplementary Fig. 13: Flammability of different electrolytes using 30 μL of solution to soak the substrate, where images are taken at 0.5 seconds after ignition (Supplementary Videos 1-4). It is seen that EL2-5 have much reduced flammability compared to the conventional 1 M $LiPF_6$ EC-DMC (3:7) electrolyte.

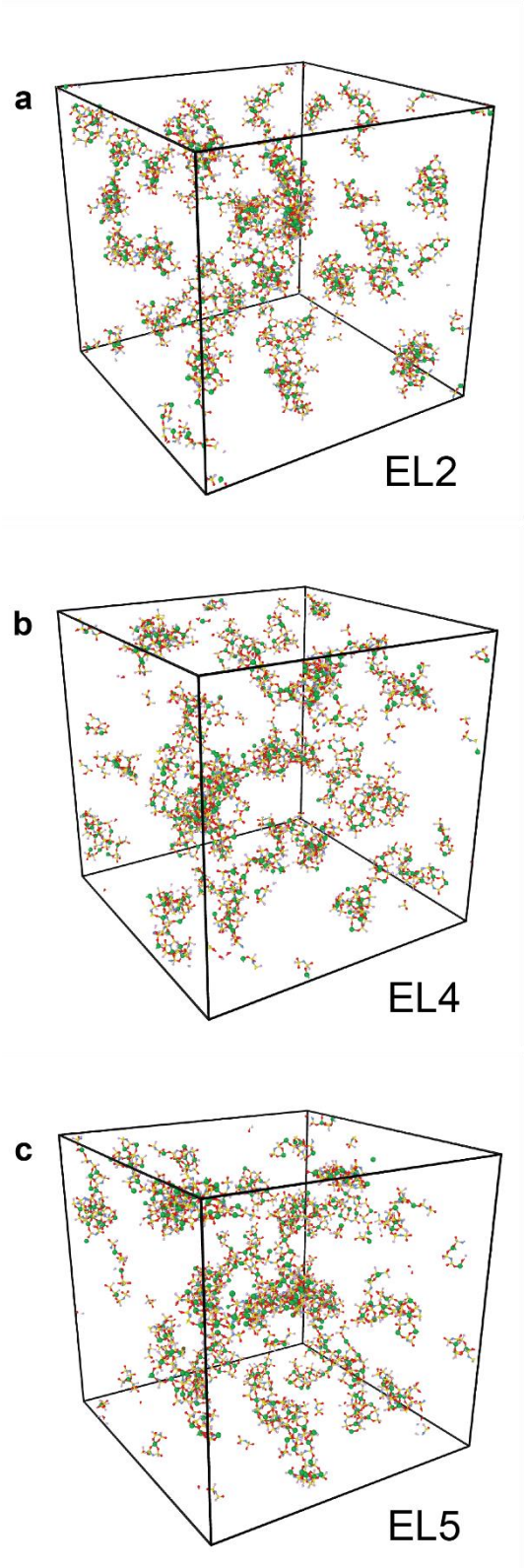


Supplementary Fig. 14: Molecular dynamics simulations of EL2-5.

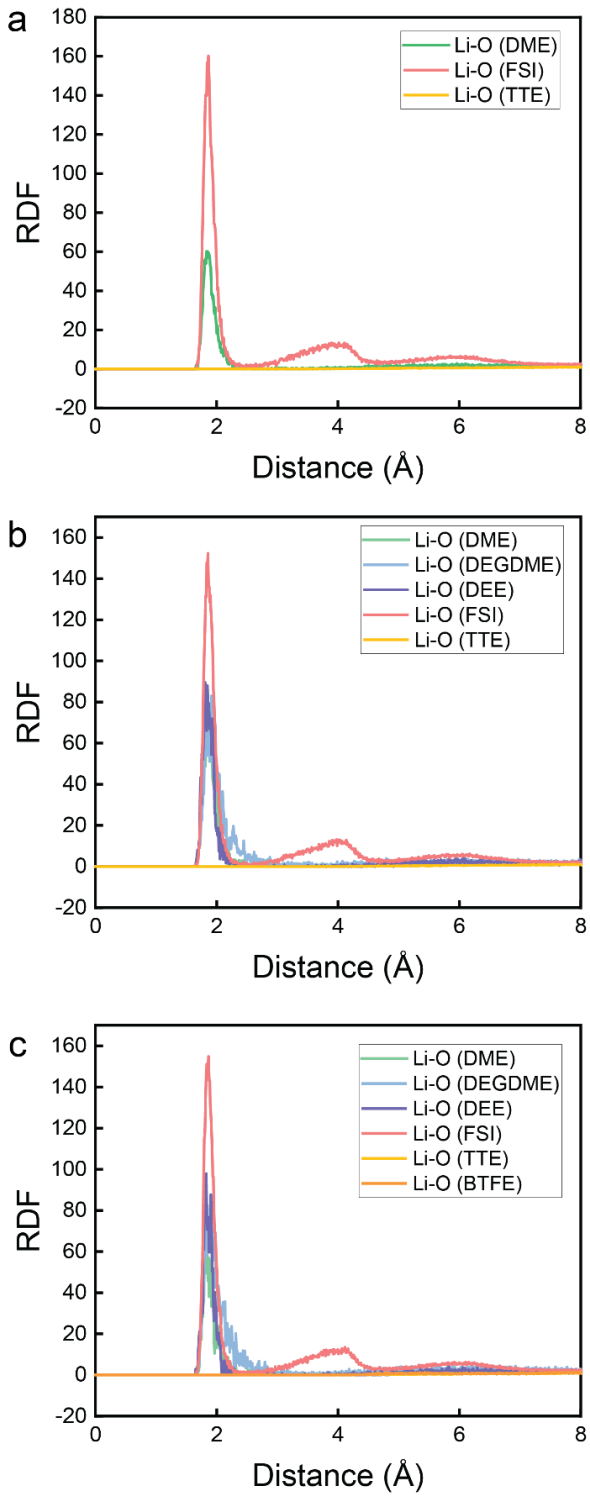


Supplementary Fig. 15: Radial distribution functions (RDFs) of $Li^+$ in a) EL2 b) EL4 c) EL5, showing the anion-rich first solvation structure.

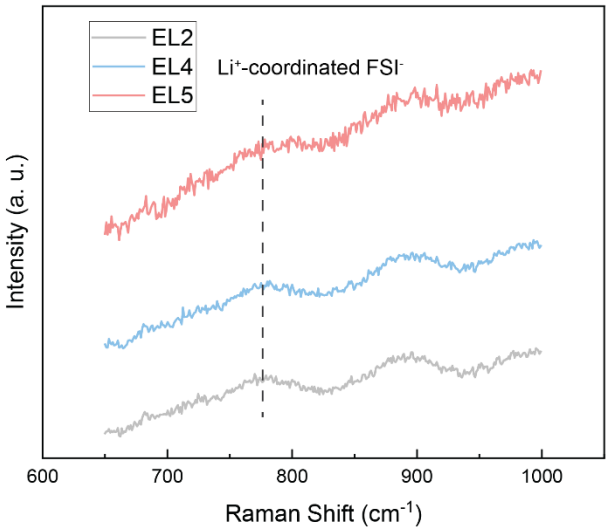


Supplementary Fig. 16. Raman spectroscopy of EL2-5, showing that the $Li^+$-coordinated $FSI^-$ shift is more or less constant across the three electrolytes.

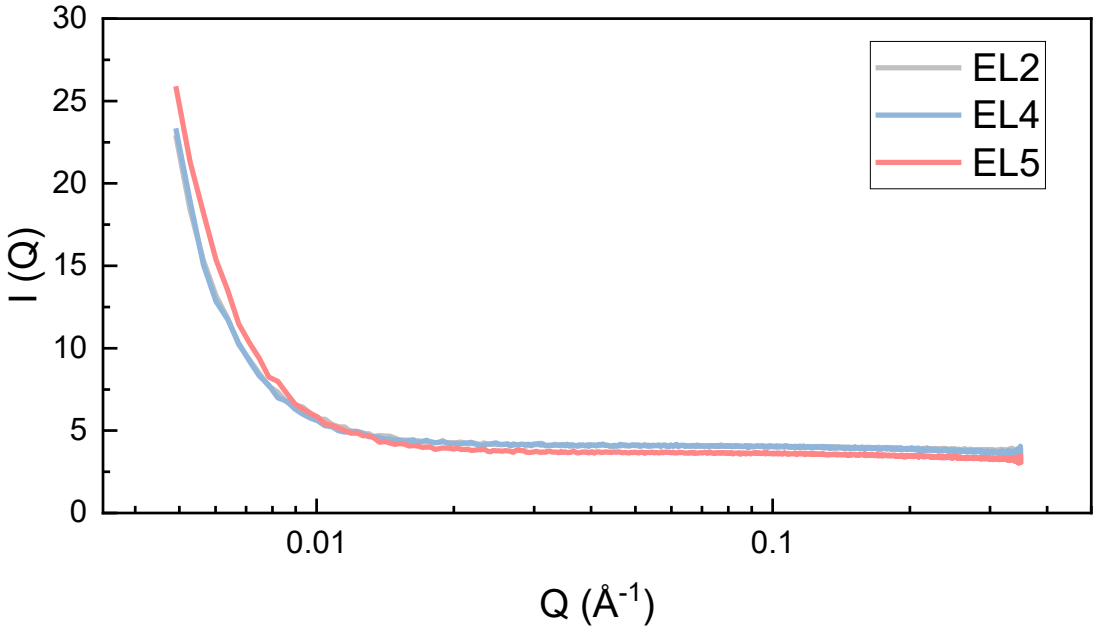


Supplementary Fig. 17: Small-angle X-ray scattering (SAXS) characterization not showing discernable differences at high Q regime.

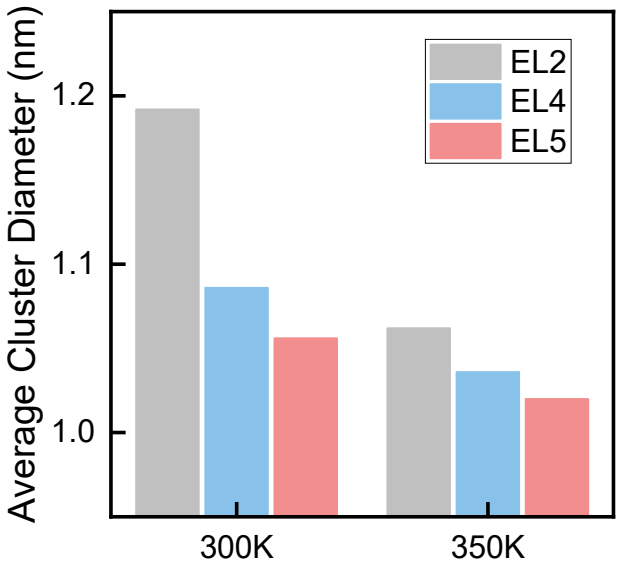


Supplementary Fig. 18: Molecular dynamics simulation of average cluster diameters for EL2-5 at 300K and 350K, where the diameters show similar trend to cluster sizes.

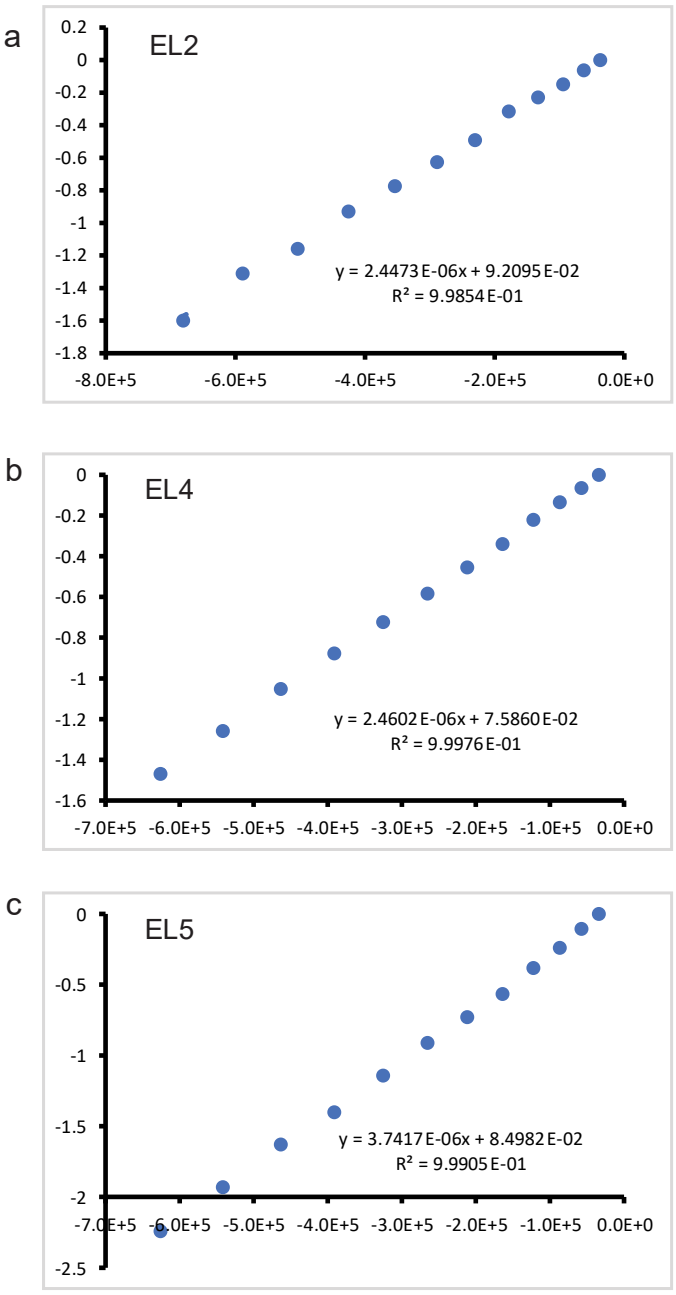


Supplementary Fig. 19: Diffusion coefficient of $Li^+$ characterized by DOSY-NMR, where the diffusion coefficients are summarized in Supplementary Table 6.

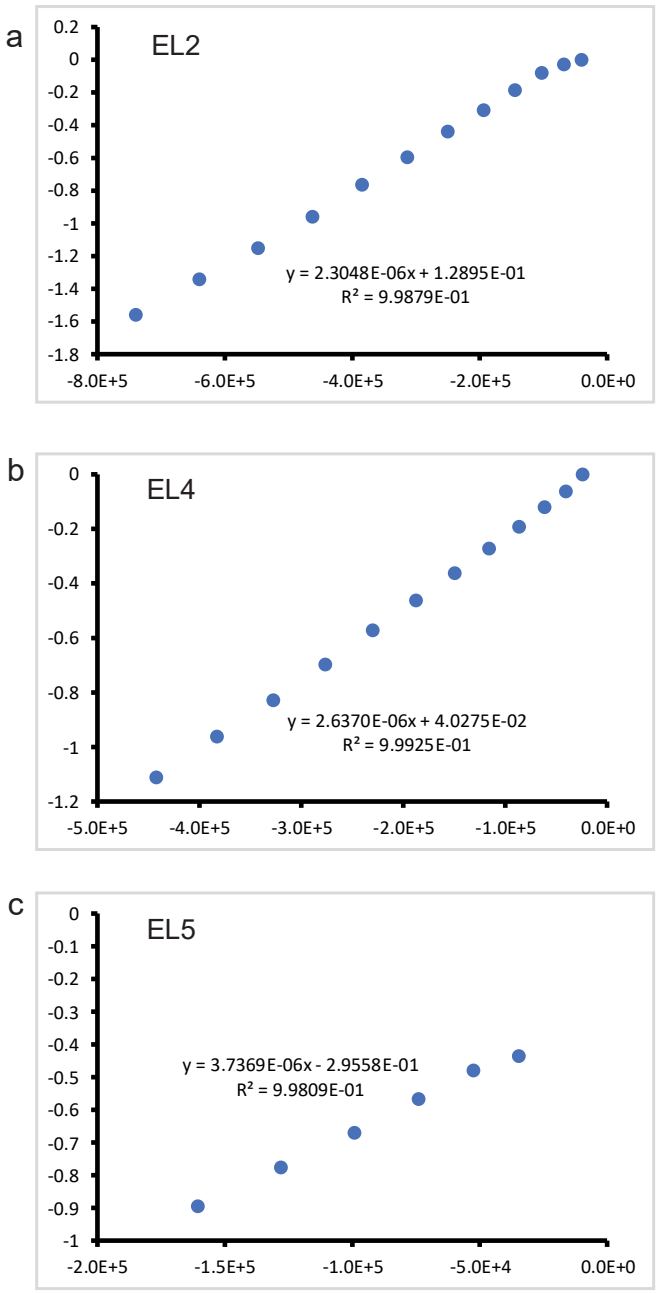


Supplementary Fig. 20: Diffusion coefficient of $FSI^-$ characterized by DOSY-NMR, where the diffusion coefficients are summarized in Supplementary Table 6.

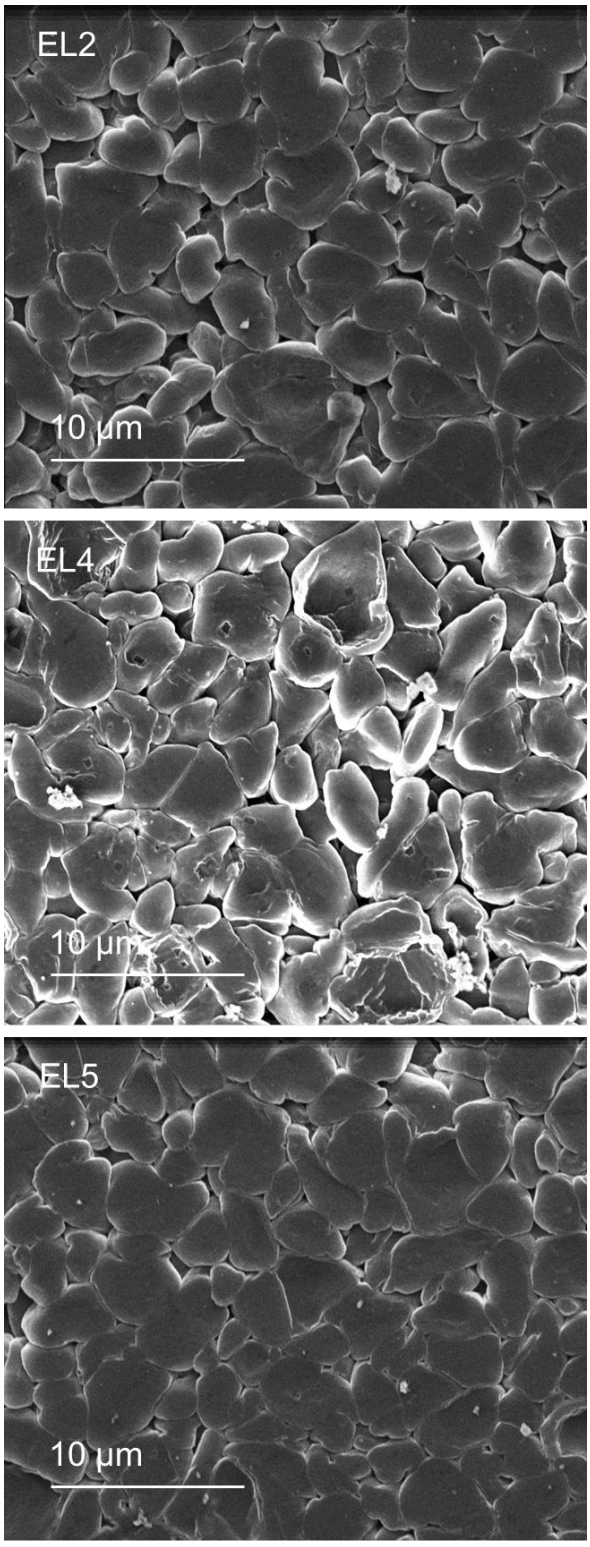


Supplementary Fig. 21: Top-view scanning electron micrographs of 1 mAh $cm^{-2}$ of Li deposited at 0.5 mA $cm^{-2}$.

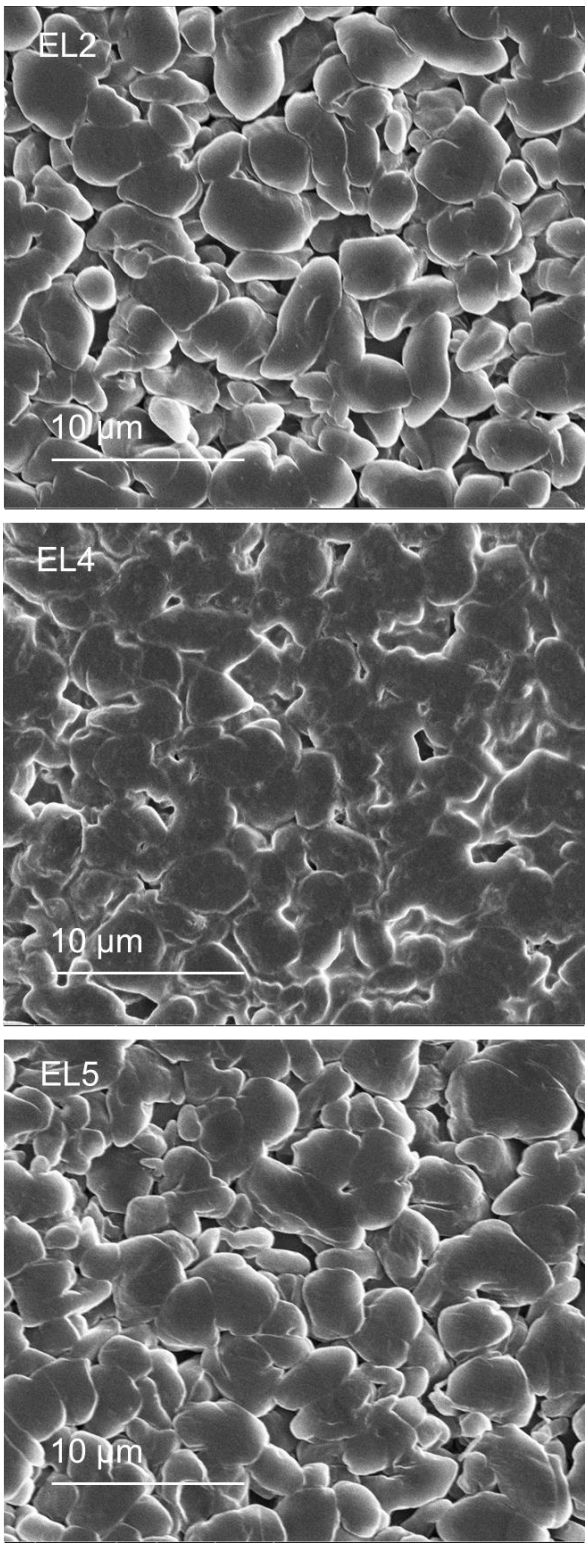


Supplementary Fig. 22: Top-view scanning electron micrographs of 1 mAh $cm^{-2}$ of Li deposited at 1 mA $cm^{-2}$.

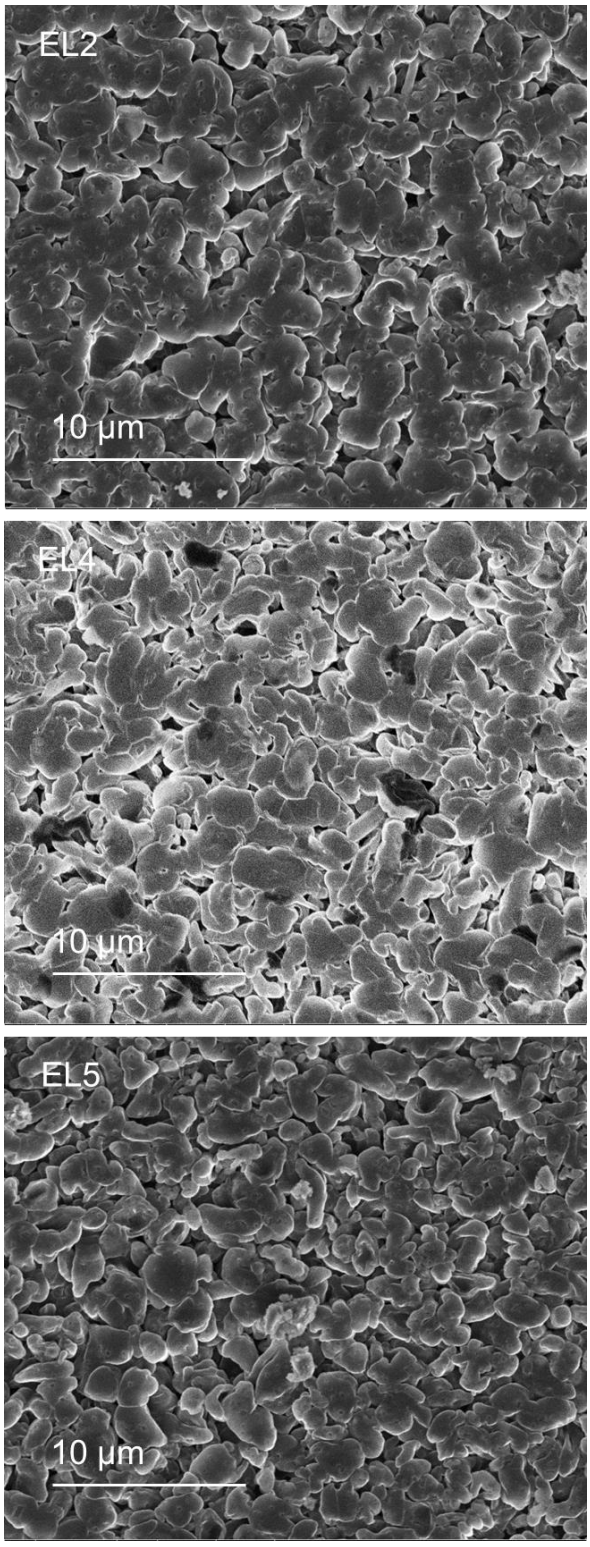


Supplementary Fig. 23: Top-view scanning electron micrographs of 1 mAh $cm^{-2}$ of Li deposited at 3 mA $cm^{-2}$.

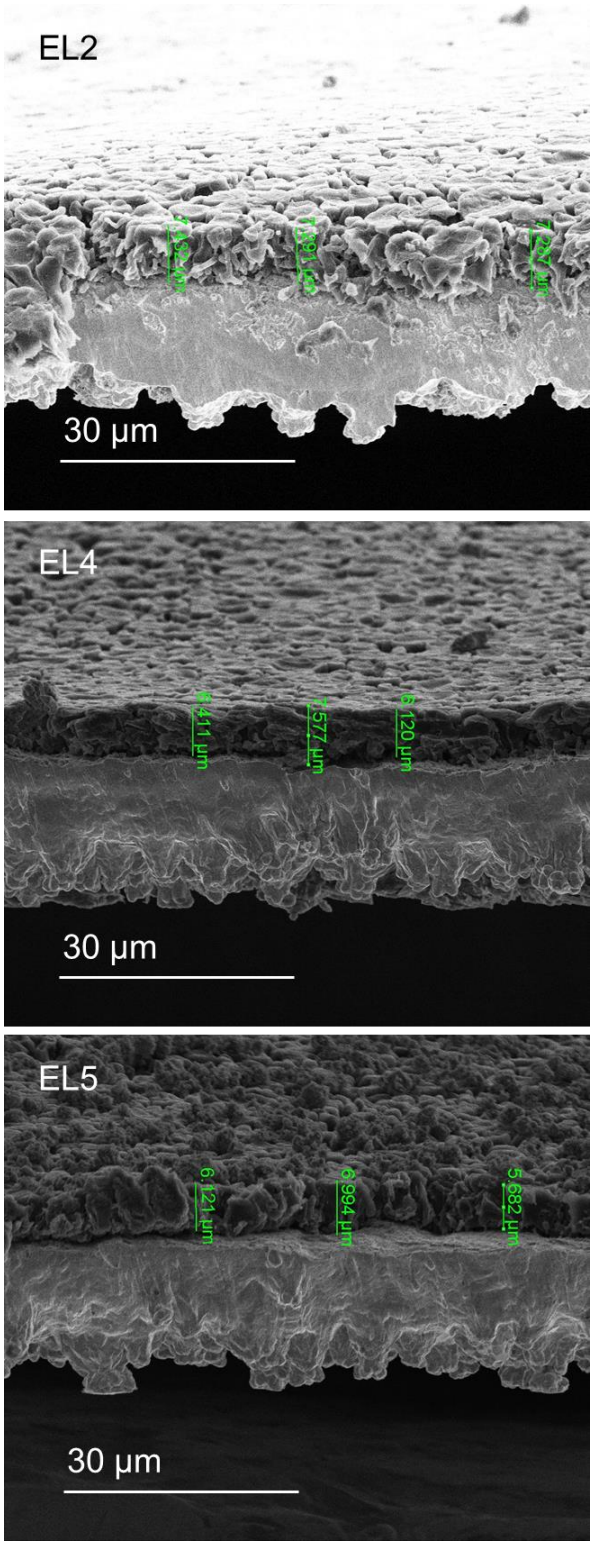


Supplementary Fig. 24: Cross-section-view scanning electron micrographs of 1 mAh $cm^{-2}$ of Li deposited at 0.5 mA $cm^{-2}$.

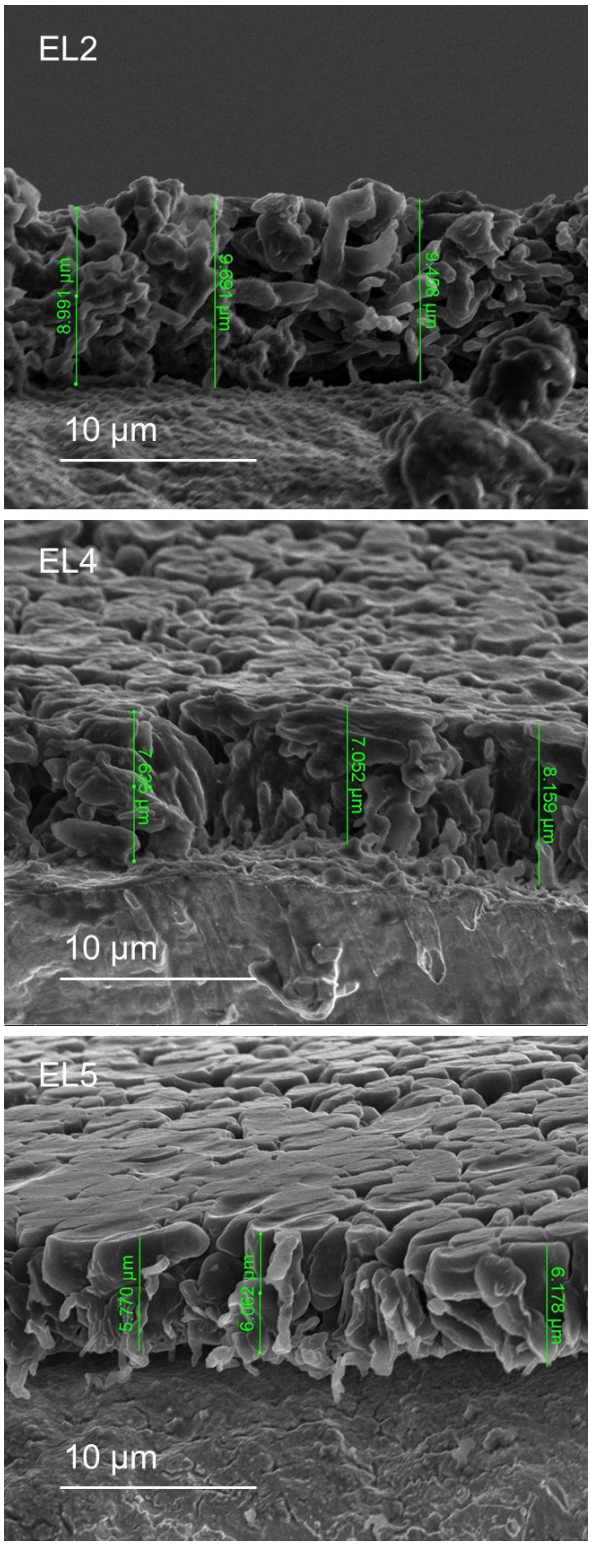


Supplementary Fig. 25: Cross-section-view scanning electron micrographs of 1 mAh $cm^{-2}$ of Li deposited at 1 mA $cm^{-2}$.

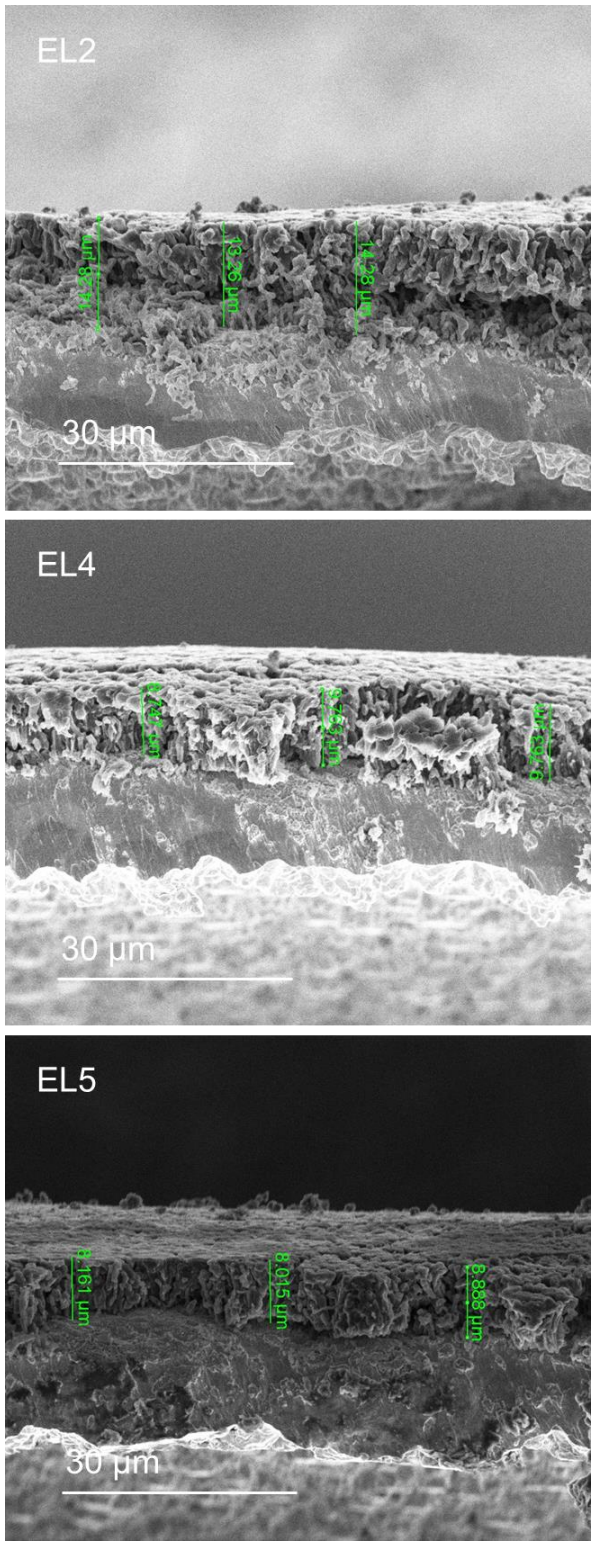


Supplementary Fig. 26: Cross-section-view scanning electron micrographs of 1 mAh $cm^{-2}$ of Li deposited at 3 mA $cm^{-2}$.

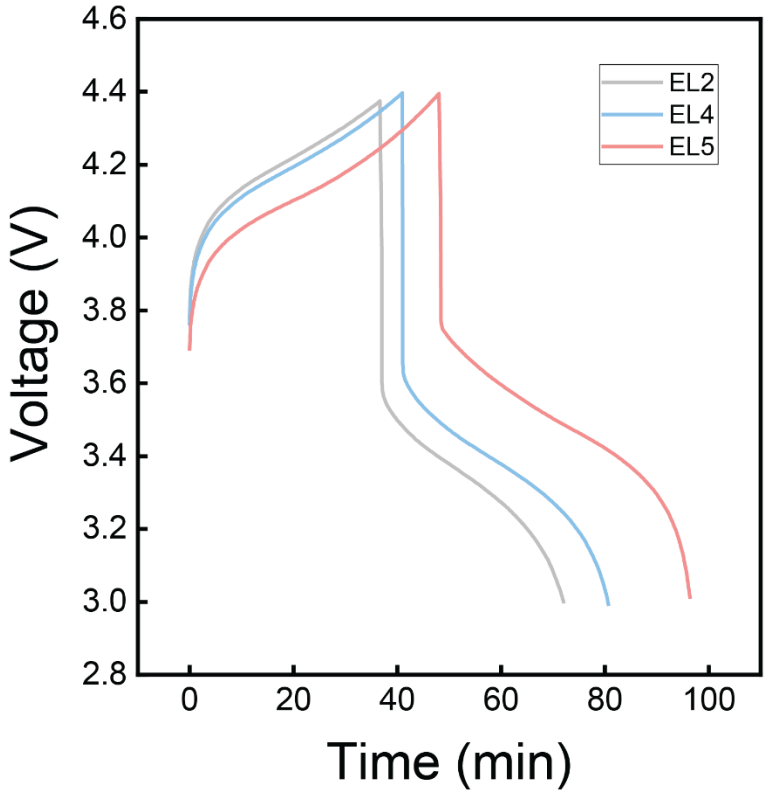


Supplementary Fig. 27: Multiphysics simulated voltage profiles of the pouch cell cycling at 1C, showing that EL5 has the smallest overpotential and highest discharge capacity.

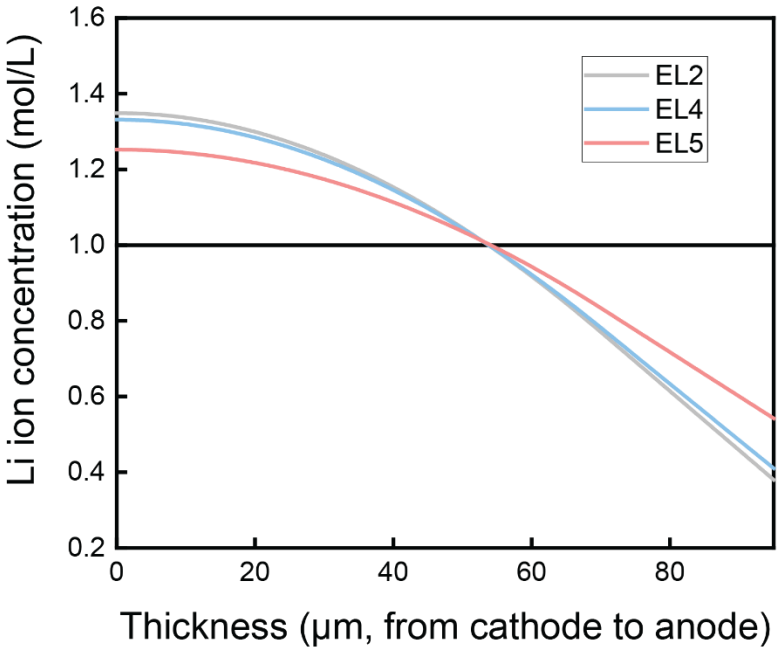


Supplementary Fig. 28: Multiphysics simulations of $Li^+$ concentration profile in the electrolyte of the pouch cell cycling at 1C charging, illustrating that EL5 has the mildest gradient while EL2 has the steepest.

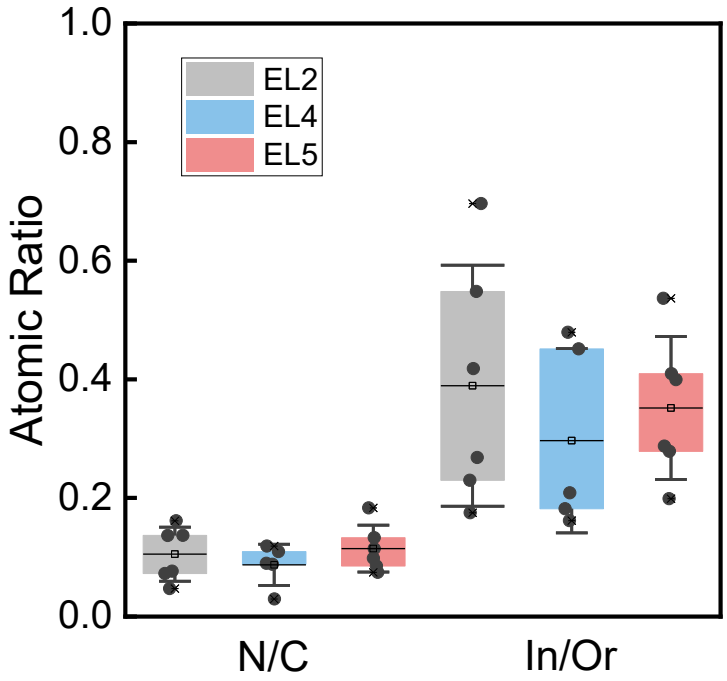


Supplementary Fig. 29: Elemental analysis from x-ray photoelectron spectroscopy (XPS) of the SEI formed in the EL2-EL5 shows that the three SEIs are compositionally similar. The horizontal lines signify the mean and the error bars are standard deviations.

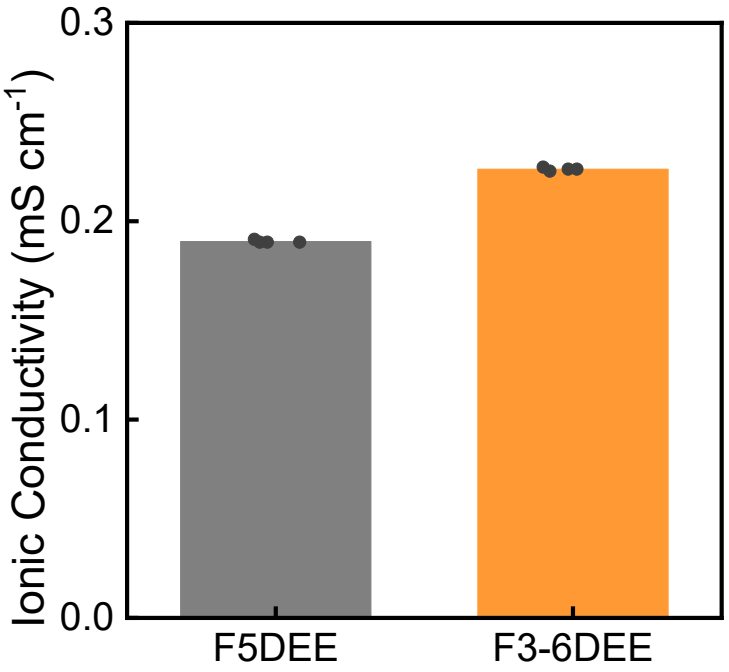


Supplementary Fig. 30: Ionic conductivities of F5DEE and F3-6DEE electrolytes measured with separators in coin cells.

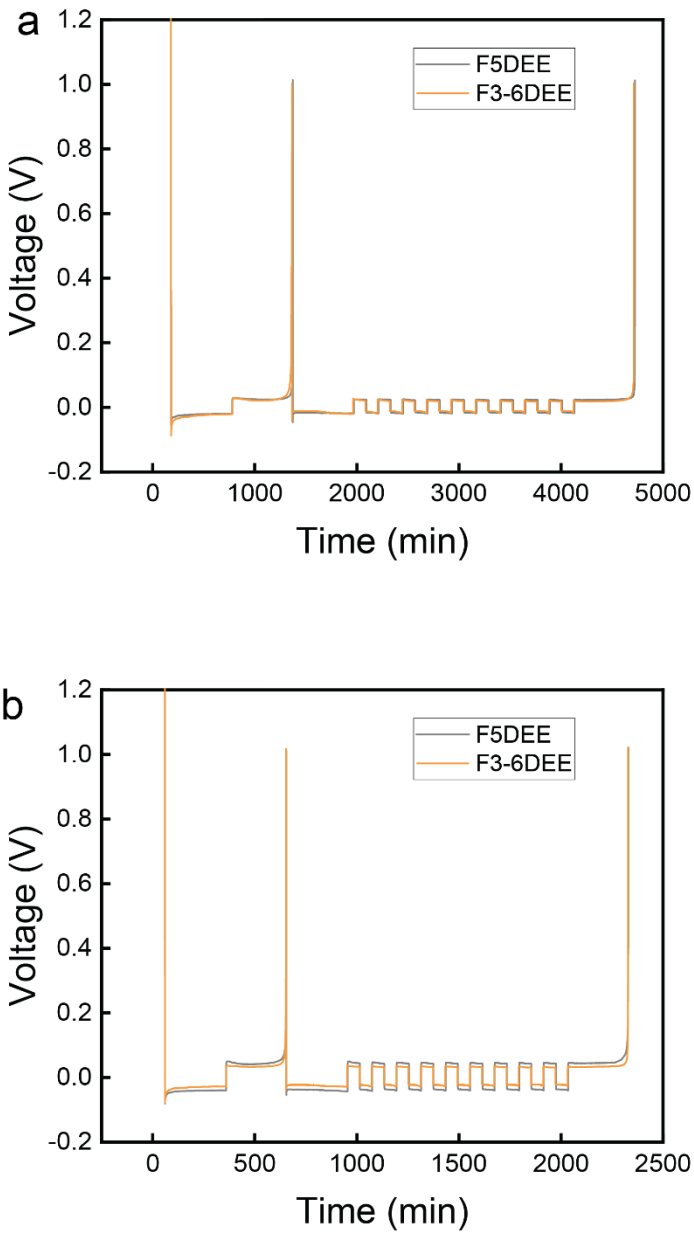


Supplementary Fig. 31: Li || Cu Coulombic efficiency measurements of F5DEE and F3-6DEE using the Aurbach method at a) 0.5 mA $cm^{-2}$ and b) 1 mA $cm^{-2}$

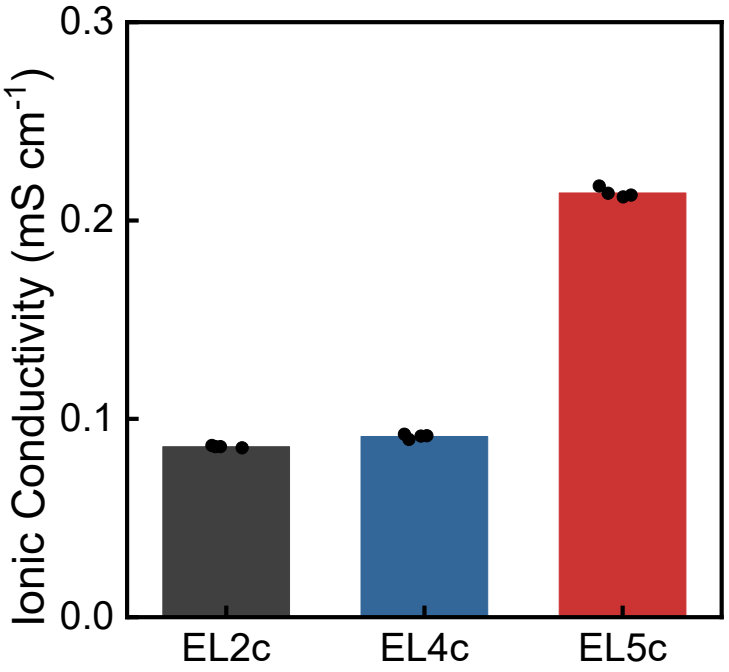


Supplementary Fig. 32: Ionic conductivities of EL2c-EL5c measured with separators in coin cells.

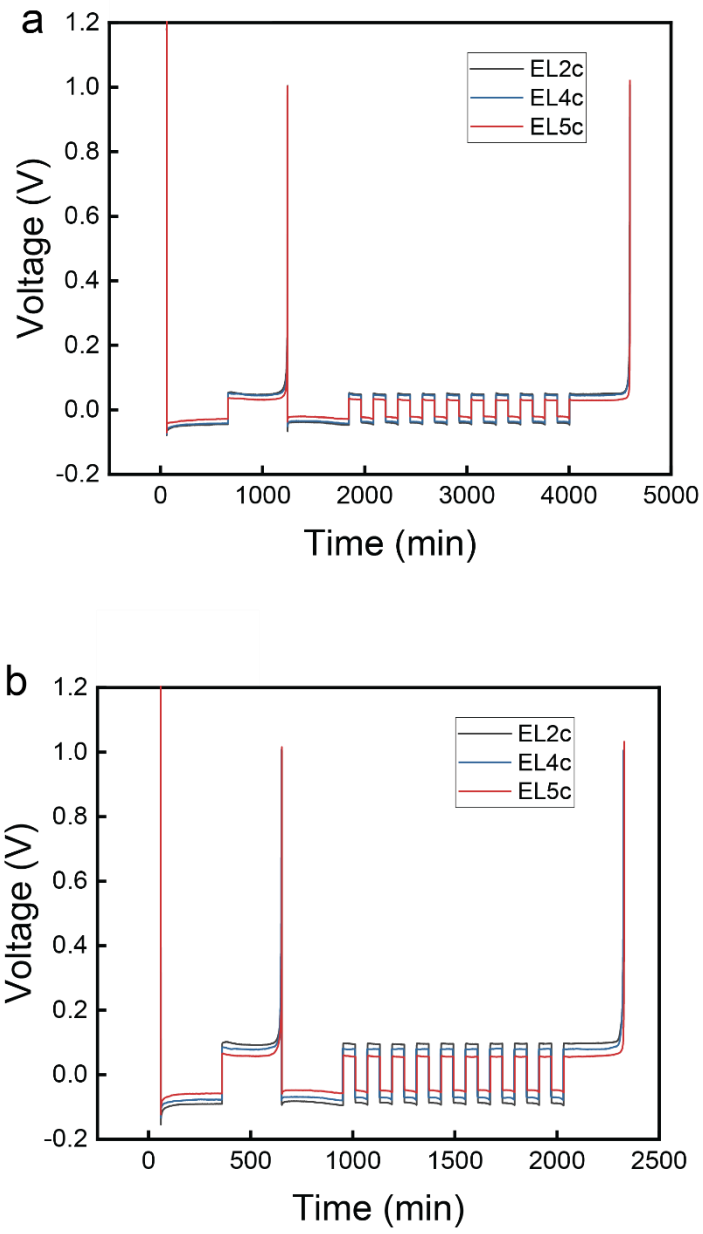


Supplementary Fig. 33: Li || Cu Coulombic efficiency measurements EL2c-EL5c using the Aurbach method at a) 0.5 mA $cm^{-2}$ and b) 1 mA $cm^{-2}$.

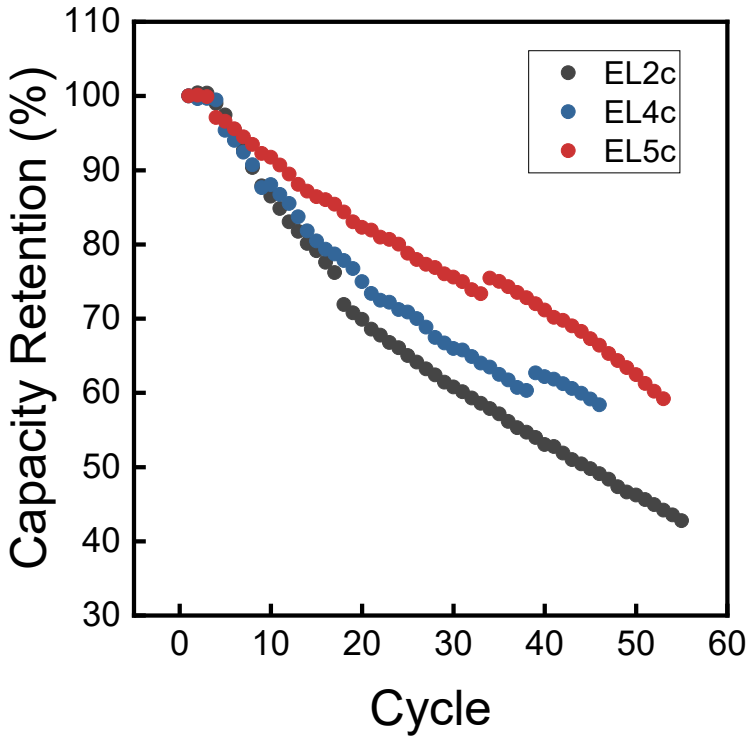


Supplementary Fig. 34: NMC532-Cu coin cell cycling of EL2c-EL5c at 1 mA $cm^{-2}$ charging and discharging currents.

**Supplementary Tables**

**Supplementary Table 1: Physical properties of electrolytes from the literature**

| Class | Electrolyte | Ionic conductivity (mS $cm^{-1}$) | Viscosity (mPa s) | References |
|---|---|---|---|---|
| Carbonate | 1 M LiPF6 EC-EMC | 10.67 | 3.5 | Chen, *Adv. Mater.* **30**, 1706102 (2018)[1] |
| Carbonate | 1 M LiPF6 EC-DMC | 11.4 | 2.01 | Berhaut, *RSC Adv.* **9**, 4599–4608 (2019)[2] |
| Carbonate | 1 M LiPF6 EC-DEC | 7.9 | 4.6 | Lundgren, *J. Electrochem. Soc.* **162**, A413–A420 (2014)[3] |
| HCE | LiFSI-1.1DMC | 1 | 180 | Chen, *Adv. Mater.* **30**, 1706102 (2018)[1] |
| HCE | LiFSI-3TMS | 1.74 | 99.5 | Ren, *Chem* **4**, 1877–1892 (2018)[4] |
| HCE | 4.2 M LiTFSI AN | 0.98 | 138.3 | Yamada, *J. Am. Chem. Soc.* **136**, 5039–5046 (2014)[5] |
| LHCE | LiFSI-2DMC-4BTFE | 2.67 | 2.7 | Chen, *Adv. Mater.* **30**, 1706102 (2018)[1] |
| LHCE | 1 M LiFSI DME-TFEO | 1.5 | 4.8 | Cao, *Nat. Energy* **4**, 796–805 (2019)[6] |
| LHCE | 1LiFSI 1.4TEP-3TTE | 0.93 | 5 | Ren, *Proc. Natl. Acad. Sci.* **117**, 28603–28613 (2020)[7] |
| LHCE | LiFSI-3TMS-3TTE | 2.03 | 14.1 | Ren, *Chem* **4**, 1877–1892 (2018)[4] |
| LHCE | LiFSI-2.2DMC-3TTE | 0.96 | 4.8 | Ren, *Proc. Natl. Acad. Sci.* **117**, 28603–28613 (2020)[7] |
| LHCE | LiFSI-1DME-3TTE | 1.59 | 3.7 | Ren, *Chem* **4**, 1877–1892 (2018)[4] |
| Ether | 1 M LiTFSI DME | 16.4 | 0.69 | Yu, *Nat. Energy* **5**, 526–533 (2020)[8] |
| Ether | 1.2 M LiFSI DME | 11 | 1.46 | Yu, *Nat. Energy* **7**, 94-106 (2022)[9] |
| Ether | 1 M LiTFSI DOL-DME | 8.9 | 3.4 | Zheng, *Adv. Energy Mater.* **9**, 1803774 (2019)[10] |
| Sulfoamide | 1 M LiFSI DMTMSA | 1.37 | 4.4 | Xue, *Nat. Energy* **6**, 495-505 (2021)[11] |
| Fluorinated ether | 1 M LiFSI FDMB | 3.5 | 5 | Yu, *Nat. Energy* **7**, 94-106 (2022)[9] |
| Fluorinated ether | 1 M LiTFSI FDMB | 3 | 4.5 | Yu, *Nat. Energy* **7**, 94-106 (2022)[9] |
| Fluorinated ether | 1.2 M F4DEE | 4.76 | 6.97 | Yu, *Nat. Energy* **7**, 94-106 (2022)[9] |
| Fluorinated ether | 1.2 M F5DEE | 5.01 | 3.39 | Yu, *Nat. Energy* **7**, 94-106 (2022)[9] |
| Fluorinated ether | 1.2 M F6DEE | 4.48 | 3.61 | Yu, *Nat. Energy* **7**, 94-106 (2022)[9] |

**Supplementary Table 2: Reported anode-free cycling of various electrolytes from the literature**

| Current Density (mA $cm^{-2}$) | Cycle | Reference |
|---|---|---|
| 0.42 | 25 | Ren, *Joule* **3**, 1662–1676 (2019)[12] |
| 0.42 | 70 | Ren, *Joule* **3**, 1662–1676 (2019)[12] |
| 0.4 | 100 | Niu, *Nat. Energy* **6**, 723–732 (2021)[13] |
| 0.58 | 200 | Louli, *Nat. Energy* **5**, 693–702 (2020)[14] |
| 0.58 | 130 | Louli, *Nat. Energy* **5**, 693–702 (2020)[14] |
| 0.48 | 90 | Weber, *Nat. Energy* **4**, 683–689 (2019)[15] |
| 0.62 | 100 | Yu, *Nat. Energy* **5**, 526–533 (2020)[8] |
| 0.62 | 60 | Yu, *Nat. Energy* **7***,* 94-106 (2022)[9] |
| 0.42 | 120 | Yu, *Nat. Energy* **7***,* 94-106 (2022)[9] |
| 0.62 | 90 | Yu, *Nat. Energy* **7***,* 94-106 (2022)[9] |
| 0.6 | 40 | Louli, *J. Electrochem. Soc.* **166**, A1291–A1299 (2019)[16] |
| 0.4 | 120 | Wang, *Adv. Mater.* **33**, 2008619 (2021)[17] |
| 0.58 | 195 | Genovese, *J. Electrochem. Soc.* **166**, A3342–A3347 (2019)[18] |

**Supplementary Table 3: Ether-based LHCE electrolyte composition**

| | Salt | Solvent | Diluent |
|---|---|---|---|
| EL2 | 1 M LiFSI | DME (10% v/v) | TTE (90% v/v) |
| EL4 | 1 M LiFSI | DME (5% v/v)<br>DEE (2.5% v/v)<br>DEGDME (2.5% v/v) | TTE (90% v/v) |
| EL5 | 1 M LiFSI | DME (5% v/v)<br>DEE (2.5% v/v)<br>DEGDME (2.5% v/v) | TTE (45% v/v)<br>BTFE (45% v/v) |

**Supplementary Table 4: Coulombic efficiency measurements**

| | | | | |
|---|---|---|---|---|
| 0.5 mA $cm^{-2}$ | EL2 | 99.44 | 99.56 | 99.50 |
| | EL4 | 99.44 | 99.33 | 99.58 |
| | EL5 | 99.50 | 99.67 | 99.55 |
| | F5DEE | 99.61 | 99.61 | 99.35 |
| | F3-6DEE | 99.60 | 99.44 | 99.70 |
| | EL2c | 99.42 | 99.56 | 99.61 |
| | EL4c | 99.49 | 99.39 | 99.49 |
| | EL5c | 99.50 | 99.55 | 99.56 |
| 1 mA $cm^{-2}$ | EL2 | 96.97 | 96.94 | 97.33 |
| | EL4 | 98.66 | 98.77 | 99.25 |
| | EL5 | 99.35 | 99.46 | 99.38 |
| | F5DEE | 99.38 | 99.43 | 99.45 |
| | F3-6DEE | 99.50 | 99.49 | 99.45 |
| | EL2c | 99.15 | 99.19 | 98.78 |
| | EL4c | 99.45 | 99.37 | 99.35 |
| | EL5c | 99.48 | 99.42 | 99.44 |

**Supplementary Table 5: Anode-free pouch cell information**

| Information | Cu \|\| single-crystal NMC532 |
|---|---|
| Cu foil thickness | 8 μm |
| Al foil thickness | 12 μm |
| Separator thickness | 12 μm PE coated with alumina |
| Package foil thickness | ~80 μm |
| Active material : carbon : binder | 94 : 4 : 2 |
| Areal capacity | ~3.1 mAh $cm^{-2}$ |
| Total capacity | 200 mAh (0.3C discharge) |
| Electrolyte/cathode ratio (E/C, g $Ah^{-1}$) | 2.4 |

**Supplementary Table 6: Diffusivity measurements from DOSY-NMR**

| Sample | $D_{Li+}$ ($cm^2\ s^{-1}$) | $D_{FSI-}$ ($cm^2\ s^{-1}$) |
|---|---|---|
| EL2 | 2.45E-06 | 2.30E-06 |
| EL4 | 2.46E-06 | 2.64E-06 |
| EL5 | 3.74E-06 | 3.74E-06 |

**Supplementary Table 7: Electrode cross-section thickness measurements by SEM in µm**

| | 0.5 mA $cm^{-2}$ | | | 1 mA $cm^{-2}$ | | | 3 mA $cm^{-2}$ | | |
|---|---|---|---|---|---|---|---|---|---|
| | **EL2** | **EL4** | **EL5** | **EL2** | **EL4** | **EL5** | **EL2** | **EL4** | **EL5** |
| **AVG** | **7.61** | **7.31** | **7.11** | **8.62** | **7.20** | **7.13** | **11.30** | **8.39** | **8.38** |
| **STDEV** | **1.40** | **1.14** | **1.23** | **2.17** | **0.65** | **1.43** | **2.30** | **0.70** | **0.79** |
| 1 | 9.179 | 6.848 | 8.888 | 8.512 | 7.635 | 6.653 | 14.13 | 8.305 | 9.908 |
| 2 | 9.621 | 6.848 | 7.432 | 9.383 | 7.052 | 7.782 | 13.41 | 7.88 | 9.908 |
| 3 | 9.034 | 7.139 | 7.724 | 8.742 | 8.159 | 7.531 | 12.24 | 8.026 | 10.05 |
| 4 | 7.869 | 6.272 | 8.451 | 12.36 | 6.604 | 11.548 | 14.76 | 6.557 | 8.161 |
| 5 | 8.306 | 6.704 | 8.742 | 12.18 | 7.547 | 6.242 | 13.02 | 7.287 | 8.015 |
| 6 | 7.724 | 6.413 | 10.2 | 12.53 | 7.17 | 6.575 | 13.41 | 8.161 | 8.888 |
| 7 | 7.432 | 8.452 | 7.868 | 6.528 | 8.585 | 5.192 | 8.451 | 7.437 | 8.015 |
| 8 | 7.291 | 8.451 | 8.014 | 6.469 | 7.285 | 5.77 | 8.014 | 8.306 | 7.145 |
| 9 | 7.287 | 8.596 | 8.742 | 7.636 | 7.286 | 6.062 | 9.325 | 8.598 | 7.432 |
| 10 | 8.014 | 8.742 | 5.684 | 8.991 | 7.81 | 6.178 | 14.28 | 8.452 | 9.035 |
| 11 | 9.035 | 8.596 | 5.974 | 9.691 | 6.412 | 6.411 | 13.26 | 8.899 | 8.159 |
| 12 | 8.742 | 7.141 | 5.682 | 9.458 | 6.061 | 6.76 | 14.28 | 8.888 | 8.596 |
| 13 | 8.601 | 7.577 | 5.83 | 6.21 | 7.111 | 6.119 | 9.035 | 8.452 | 8.598 |
| 14 | 8.889 | 6.85 | 5.83 | 7.021 | 6.604 | 7.601 | 9.471 | 8.888 | 7.868 |
| 15 | 8.743 | 6.411 | 5.682 | 5.979 | 6.608 | 8.023 | 9.179 | 9.035 | 8.306 |
| 16 | 9.908 | 9.034 | 6.121 | 6.287 | 7.012 | 8.659 | 8.742 | 8.015 | 7.869 |
| 17 | 8.451 | 9.325 | 6.413 | | 6.62 | 8.058 | 9.471 | 8.743 | 7.869 |
| 18 | 9.034 | 9.179 | 5.684 | | 8.058 | | 8.161 | 8.452 | 7.285 |
| 19 | 6.12 | 6.12 | 5.83 | | | | 10.93 | 7.869 | 8.015 |
| 20 | 5.399 | 5.1 | 6.121 | | | | 12.09 | 8.015 | 8.161 |
| 21 | 5.247 | 5.393 | 6.994 | | | | 11.66 | 7.722 | 8.596 |
| 22 | 5.247 | 6.411 | 5.682 | | | | | 8.888 | |
| 23 | 5.539 | 7.577 | 7.578 | | | | | 9.18 | |
| 24 | 5.835 | 6.12 | 7.868 | | | | | 8.161 | |
| 25 | 7.868 | 6.848 | 7.868 | | | | | 8.787 | |
| 26 | 7.728 | 6.267 | 7.577 | | | | | 9.763 | |
| 27 | 6.704 | 6.267 | 7.287 | | | | | 9.763 | |
| 28 | 5.537 | 7.868 | 7.432 | | | | | | |
| 29 | 6.411 | 8.452 | | | | | | | |
| 30 | | 8.159 | | | | | | | |

**Supplementary Table 8: FDEE based electrolyte compositions**

| Name | Salt | Solvent |
|---|---|---|
| F5DEE | 1 M LiFSI | F5DEE |
| F3-6DEE | 1 M LiFSI | F3DEE (25% v/v)<br>F4DEE (25% v/v)<br>F5DEE (25% v/v)<br>F6DEE (25% v/v) |

**Supplementary Table 9: Carbonate based LHCE electrolyte compositions**

| | Salt | Solvent | Diluent |
|---|---|---|---|
| EL2c | 1 M LiFSI | EMC (15% v/v) | TTE (85% v/v) |
| EL4c | 1 M LiFSI | EMC (7.5% v/v)<br>DMC (3.75% v/v)<br>DEC (3.75% v/v) | TTE (85% v/v) |
| EL5c | 1 M LiFSI | EMC (7.5% v/v)<br>DMC (3.75% v/v)<br>DEC (3.75% v/v) | TTE (42.5% v/v)<br>BTFE (42.5% v/v) |

**Supplementary Table 10: OPLS-AA parameters for 1,1,2,2-tetrafluoroethyl-2,2,3,3-tetrafluoropropyl ether (TTE)**

| Atom type | ε (kcal/mol) | σ (Å) | Q (e) |
|---|---|---|---|
| F2 | 0.060 | 2.90 | -0.15 |
| F3 | 0.060 | 2.90 | -0.16 |
| O1 | 0.210 | 2.96 | -0.16 |
| C1 | 0.066 | 3.50 | 0.25 |
| C2 | 0.066 | 3.50 | -0.08 |
| C3 | 0.066 | 3.50 | 0.25 |
| C4 | 0.066 | 3.50 | 0.25 |
| H1 | 0.030 | 2.50 | 0.12 |

| Bond type | $k_r$ (kcal/mol·Å$^2$) | $r_0$ (Å) |
|---|---|---|
| F2-C1 | 413.500 | 1.36 |
| C3-C4 | 319.000 | 1.53 |
| F2-C3 | 367.000 | 1.36 |
| C4-H1 | 388.500 | 1.10 |
| O1-C2 | 360.000 | 1.42 |
| O1-C3 | 455.000 | 1.34 |
| C1-C2 | 325.000 | 1.51 |
| F3-C4 | 430.000 | 1.35 |
| C2-H1 | 385.500 | 1.10 |
| C1-C4 | 305.500 | 1.53 |

| Angle type | $k_\theta$ (kcal/mol·rad$^2$) | $\theta_0$ (deg) |
|---|---|---|
| F2-C1-C2 | 92.00 | 110.42 |
| F2-C1-C4 | 88.00 | 108.00 |
| F2-C1-F2 | 119.00 | 107.79 |
| F2-C1-C2 | 92.00 | 110.18 |
| C2-C1-C4 | 82.00 | 112.29 |
| O1-C2-C1 | 87.00 | 106.66 |
| O1-C2-H1 | 69.00 | 110.81 |
| C1-C2-H1 | 54.00 | 109.28 |
| H1-C2-H1 | 49.00 | 109.93 |
| O1-C3-C4 | 89.00 | 110.70 |
| F2-C3-O1 | 120.50 | 111.90 |
| F2-C3-F2 | 123.00 | 105.50 |
| F2-C3-C4 | 84.00 | 108.39 |
| F2-C3-O1 | 119.00 | 111.74 |
| F3-C4-C1 | 87.50 | 109.04 |
| F3-C4-F3 | 116.00 | 108.67 |
| C1-C4-H1 | 71.00 | 109.50 |
| C3-C4-H1 | 87.50 | 109.08 |
| C2-O1-C3 | 56.00 | 111.66 |

| Dihedral type | $V_1$ (kcal/mol) | $V_2$ (kcal/mol) | $V_3$ (kcal/mol) |
|---|---|---|---|
| C3-O1-C2-C1 | 1.629 | 0.311 | 0.028 |

| | | | |
|---|---|---|---|
| C3-O1-C2-H1 | -1.659 | -0.280 | -0.050 |
| C2-O1-C3-F2 | -1.713 | -0.414 | -0.731 |
| C2-O1-C3-C4 | 1.590 | 0.611 | -0.104 |
| F2-C1-C2-O1 | -0.403 | 0.270 | -0.606 |
| F2-C1-C2-H1 | 0.242 | -0.310 | 0.914 |
| C4-C1-C2-O1 | 0.644 | 0.556 | 0.515 |
| C4-C1-C2-H1 | -0.493 | 0.525 | 1.191 |
| F2-C1-C4-F3 | -0.129 | -0.144 | -0.109 |
| F2-C1-C4-H1 | 0.102 | 0.131 | -0.150 |
| C2-C1-C4-F3 | 0.151 | 0.168 | -0.274 |
| C2-C1-C4-H1 | -0.125 | -0.154 | -0.183 |
| F2-C3-C4-F3 | 0.291 | 0.048 | -0.224 |
| F2-C3-C4-H1 | -0.254 | -0.067 | -0.023 |
| O1-C3-C4-F3 | -0.264 | -0.061 | -0.244 |
| O1-C3-C4-H1 | 0.229 | 0.083 | -0.076 |

**Supplementary Table 11. Transport properties of different electrolytes used in the numerical modeling**

| | EL2 | EL4 | EL5 |
|---|---|---|---|
| Ionic conductivity (mS/cm) | 1.67 | 1.89 | 3.57 |
| Transference number | 0.247 | 0.229 | 0.229 |
| $Li^+$ diffusion coefficient ($cm^2/s$) | $2.45\times10^{-6}$ | $2.46\times10^{-6}$ | $3.74\times10^{-6}$ |

**Supplementary Table 12. Other material properties used in the numerical modeling**

| Parameter (unit) | Value | Parameter (unit) | Value |
|---|---|---|---|
| Electric conductivity of carbon-binder matrix ($S \cdot m^{-1}$) | $10^4$ | Initial Li concentration in electrolyte ($mol \cdot m^{-3}$) | 1000 |
| Rate constant for cathodic reaction (m/s) | $2 \times 10^{-11}$ | Reference Li concentration for Li electrodeposition ($mol \cdot m^{-3}$) | 1000 |
| Rate constant for anodic reaction (m/s) | $2 \times 10^{-11}$ | Max. Li concentration in NMC ($mol \cdot m^{-3}$) | 48700 |
| Cathodic transfer coefficient (1) | 0.5 | Porosity of NMC cathode (1) | 0.36 |
| Anodic transfer coefficient (1) | 0.5 | Porosity of separator (1) | 0.4 |
| Li diffusivity in NMC ($m^2 \cdot s^{-1}$) | $5 \times 10^{-13}$ | Tortuosity of NMC cathode, (1) | 3 |
| Dimeter of NMC particle (μm) | 10 | Tortuosity of separator (1) | 3 |

**References**


1. Chen, S. *et al.* High-Voltage Lithium-Metal Batteries Enabled by Localized High-Concentration Electrolytes. *Adv. Mater.* **30**, 1–7 (2018).

2. Berhaut, C. L. *et al.* Ionic association analysis of LiTDI, LiFSI and LiPF6 in EC/DMC for better Li-ion battery performances. *RSC Adv.* **9**, 4599–4608 (2019).

3. Lundgren, H., Behm, M. & Lindbergh, G. Electrochemical Characterization and Temperature Dependency of Mass-Transport Properties of $LiPF_6$in EC:DEC. *J. Electrochem. Soc.* **162**, A413–A420 (2014).

4. Ren, X. *et al.* Localized High-Concentration Sulfone Electrolytes for High-Efficiency Lithium-Metal Batteries. *Chem* **4**, 1877–1892 (2018).

5. Yamada, Y. *et al.* Unusual stability of acetonitrile-based superconcentrated electrolytes for fast-charging lithium-ion batteries. *J. Am. Chem. Soc.* **136**, 5039–5046 (2014).

6. Cao, X. *et al.* Monolithic solid–electrolyte interphases formed in fluorinated orthoformate-based electrolytes minimize Li depletion and pulverization. *Nat. Energy* **4**, 796–805 (2019).

7. Ren, X. *et al.* Role of inner solvation sheath within salt–solvent complexes in tailoring electrode/electrolyte interphases for lithium metal batteries. *Proc. Natl. Acad. Sci.* **117**, 28603–28613 (2020).

8. Yu, Z. *et al.* Molecular design for electrolyte solvents enabling energy-dense and long-cycling lithium metal batteries. *Nat. Energy 2020 57* **5**, 526–533 (2020).

9. Yu, Z. *et al.* Rational solvent molecule tuning for high-performance lithium metal battery electrolytes. *Nat. Energy* (2022) doi:10.1038/s41560-021-00962-y.

10. Zheng, J. *et al.* High-Fluorinated Electrolytes for Li–S Batteries. *Adv. Energy Mater.* **9**, 1803774 (2019).

11. Xue, W. *et al.* Ultra-high-voltage Ni-rich layered cathodes in practical Li metal batteries enabled by a sulfonamide-based electrolyte. *Nat. Energy* (2021) doi:10.1038/s41560-021-00792-y.

12. Ren, X. *et al.* Enabling High-Voltage Lithium-Metal Batteries under Practical Conditions. *Joule* **3**, 1662–1676 (2019).

13. Niu, C. *et al.* Balancing interfacial reactions to achieve long cycle life in high-energy lithium metal batteries. *Nat. Energy* **6**, 723–732 (2021).

14. Louli, A. J. *et al.* Diagnosing and correcting anode-free cell failure via electrolyte and morphological analysis. *Nat. Energy* **5**, 693–702 (2020).

15. Weber, R. *et al.* Long cycle life and dendrite-free lithium morphology in anode-free lithium pouch cells enabled by a dual-salt liquid electrolyte. *Nat. Energy 2019 48* **4**, 683–689 (2019).

16. Louli, A. J. *et al.* Exploring the Impact of Mechanical Pressure on the Performance of Anode-Free Lithium Metal Cells. *J. Electrochem. Soc.* **166**, A1291–A1299 (2019).

17. Wang, H. *et al.* Dual-Solvent Li-Ion Solvation Enables High-Performance Li-Metal Batteries. *Adv. Mater.* **33**, 2008619 (2021).

18. Genovese, M. *et al.* Hot Formation for Improved Low Temperature Cycling of Anode-Free Lithium Metal Batteries. *J. Electrochem. Soc.* **166**, A3342–A3347 (2019).